Supporting Information

Complete Gaussian reference:

Gaussian 03, Revision D.02, Frisch, M. J.; Trucks, G. W.; Schlegel, H. B.; Scuseria, G. E.; Robb, M. A.; Cheeseman, J. R.; Montgomery, Jr., J. A.; Vreven, T.; Kudin, K. N.; Burant, J. C.; Millam, J. M.; Iyengar, S. S.; Tomasi, J.; Barone, V.; Mennucci, B.; Cossi, M.; Scalmani, G.; Rega, N.; Petersson, G. A.; Nakatsuji, H.; Hada, M.; Ehara, M.; Toyota, K.; Fukuda, R.; Hasegawa, J.; Ishida, M.; Nakajima, T.; Honda, Y.; Kitao, O.; Nakai, H.; Klene, M.; Li, X.; Knox, J. E.; Hratchian, H. P.; Cross, J. B.; Bakken, V.; Adamo, C.; Jaramillo, J.; Gomperts, R.; Stratmann, R. E.; Yazyev, O.; Austin, A. J.; Cammi, R.; Pomelli, C.; Ochterski, J. W.; Ayala, P. Y.; Morokuma, K.; Voth, G. A.; Salvador, P.; Dannenberg, J. J.; Zakrzewski, V. G.; Dapprich, S.; Daniels, A. D.; Strain, M. C.; Farkas, O.; Malick, D. K.; Rabuck, A. D.; Raghavachari, K.; Foresman, J. B.; Ortiz, J. V.; Cui, Q.; Baboul, A. G.; Clifford, S.; Cioslowski, J.; Stefanov, B. B.; Liu, G.; Liashenko, A.; Piskorz, P.; Komaromi, I.; Martin, R. L.; Fox, D. J.; Keith, T.; Al-Laham, M. A.; Peng, C. Y.; Nanayakkara, A.; Challacombe, M.; Gill, P. M. W.; Johnson, B.; Chen, W.; Wong, M. W.; Gonzalez, C.; and Pople, J. A.; Gaussian, Inc., Wallingford CT, 2004.

a) moment analysis

To start with the moment analysis following Mauriq and Waugh from each $^{31}$P-MAS-NMR spectrum the exact chemical shift and integral of every single spinning sideband had to be read out. In order to avoid random errors, which would have occurred if the spectra would have been integrated by hand, the spectra where deconvoluted with a Lorenz-Gauss function. In table a the resulting chemical shift and integral values for each spinning side band for the ethyltris(2-furyl)phosphonium iodide at a spinning frequency of 4000 Hz are shown.

| spinning sideband | chemical shift δ [Hz] | peak area |
|---|---|---|
| -4 | 14237.0 | 1.0 |
| -3 | 10238.5 | 11.1 |
| -2 | 6237.8 | 52.6 |
| -1 | 2239.3 | 213.4 |
| 0 | -1763.6 | 317.6 |
| 1 | -5762.1 | 176.4 |
| 2 | -9765.0 | 66.6 |
| 3 | -13765.7 | 14.5 |
| 4 | -17766.4 | 1.7 |

**Table a**. $^{31}$P-NMR chemical shift and integral values for each spinning side band of ethyltris(2-furyl)phosphonium iodide **2d** at MAS spinning frequencies of 4000 Hz.

After setting the sum of all peak areas to one, we could calculate the first three central moments $M_1$, $M_2$ and $M_3$ according to the equations:

$$M_1 = (\nu - \nu_{iso})^1 \cdot I_i = 0 \qquad \text{(I)}$$

$$M_2 = (\nu - \nu_{iso})^2 \cdot I_i = \frac{1}{15} \cdot \Delta\nu^2 \cdot (3 + \eta^2) \quad \text{(II)}$$

$$M_3 = (\nu - \nu_{iso})^3 \cdot I_i = \frac{2}{35} \cdot \Delta\nu^3 \cdot (1 - \eta^2) \quad \text{(III)}$$

Since we recorded five different MAS spectra at spinning frequencies between 4000 and 700 Hz, five sets of central moments $M_1$, $M_2$ and $M_3$ were calculated. The calculated values are shown in table b.

| spinning freq. [Hz] | $M_1$ [Hz] | $M_2$ [$Hz^2$] | $M_3$ [$Hz^3$] |
|---|---|---|---|
| 4000 | -23.9 | $21.8*10^6$ | $-16.2*10^9$ |
| 3200 | -77.1 | $21.3*10^6$ | $-19.3*10^9$ |
| 2300 | -73.7 | $21.4*10^6$ | $-21.1*10^9$ |
| 1400 | -140.5 | $21.1*10^6$ | $-24.0*10^9$ |
| 700 | -49.6 | $21.6*10^6$ | $-20.6*10^9$ |

**Table b**. The calculated central moments for the case of ethyltris(2-furyl)phosphonium iodide **2d**.

By setting the average values of the central moments $M_2$ and $M_3$ in the equation:

$$\Delta\nu^3 - \frac{15}{4} \cdot M_2 \cdot \Delta\nu - \frac{35}{8} \cdot M_3 = 0 \quad \text{(IV)}$$

we can calculate the frequency values of the three main axis components of the chemical shift. With equation

$$\delta_{ii} = \frac{\Delta\nu_{ii}}{SF01} + \delta_{iso} \quad \text{(V)}$$

we can calculate the chemical shift values from the resonance frequencies. The resulting three different chemical shift values are the three main axis chemical shift tensor elements $\delta_{11}$, $\delta_{22}$ and $\delta_{33}$, with the convention $\delta_{11} \geq \delta_{22} \geq \delta_{33}$. The result of these calculations for the ethyltris(2-furyl)phosphonium iodide **2d** is shown in table c.

| spinning freq. [Hz] | $\delta_{11}$ [ppm] | $\delta_{22}$ [ppm] | $\delta_{33}$ [ppm] |
|---|---|---|---|
| 4000 | 25.64 | -5.98 | -48.45 |
| 3200 | 24.80 | -5.18 | -48.41 |
| 2300 | 24.60 | -4.78 | -48.62 |
| 1400 | 23.86 | -4.00 | -48.66 |
| 700 | 24.92 | -4.96 | -48.76 |
| average | 24.8 | -5.0 | -48.6 |

**Table c**. The calculated main axis chemical shift tensor elements $\delta_{11}$, $\delta_{22}$, $\delta_{33}$ at each recorded MAS spinning frequency.

Following the same way the three main axis chemical shift tensor elements for each of the other three phosphonium salts could be calculated. The average values of $\delta_{11}$, $\delta_{22}$ and $\delta_{33}$ for the phosphonium salts are shown in table d.

| phosphonium salt | $\delta_{iso}$ [ppm] | $\delta_{11}$ [ppm] | $\delta_{22}$ [ppm] | $\delta_{33}$ [ppm] |
|---|---|---|---|---|
| $EtP^{+}Ph_3\ I^{-}$ | 26.9 | 42.7 | 30.9 | 7.1 |
| $EtP^{+}Ph_2Fu\ I^{-}$ | 16.3 | 39.2 | 14.7 | -5.0 |
| $EtP^{+}PhFu_2\ I^{-}$ | 4.4 | 34,2 | 14.7 | -35.7 |
| $EtP^{+}Fu_3\ I^{-}$ | -9.6 | 24.8 | -5.0 | -48.6 |
| $\Delta\delta$ | -36.5 | -17.9 | -35.9 | 55.7 |

**Table d**. The calculated main axis chemical shift tensor elements $\delta_{11}$, $\delta_{22}$, $\delta_{33}$ for the four investigated phosphonium salts together with the average change of the $^{31}$P-NMR chemical shift $\Delta\delta$.

b) crystal structures:

In figure a the crystal structure of ethyl(2-furyl)diphenylphosphonium iodide **2b** is shown.

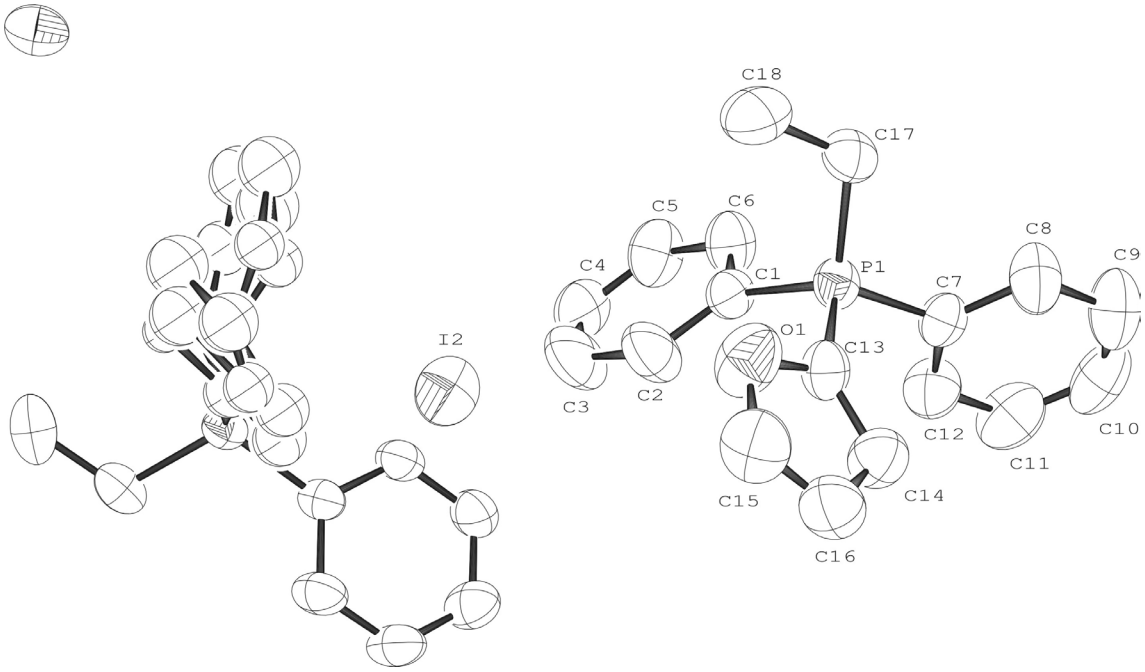


**Figure a**. Crystal structure of ethyl(2-furyl)diphenylphosphonium iodide **2b**. Two molecules are present in the unit cell. The left structure shows severe missorders as a result of random presence of 2-furyl and phenyl groups at this crystal position.

The cation crystallises in a triclinic crystal system with the space group P-1. Two molecules are present in the unit cell. In figure a it can be seen that the left structure exhibits severe missorders. This is most likely due to a random distribution of phenyl substituents and 2-furyl rings at this crystal position, which could not be resolved.

In figure b the structure of ethylbis(2-furyl)phenylphosphonium iodide **2c** is shown.

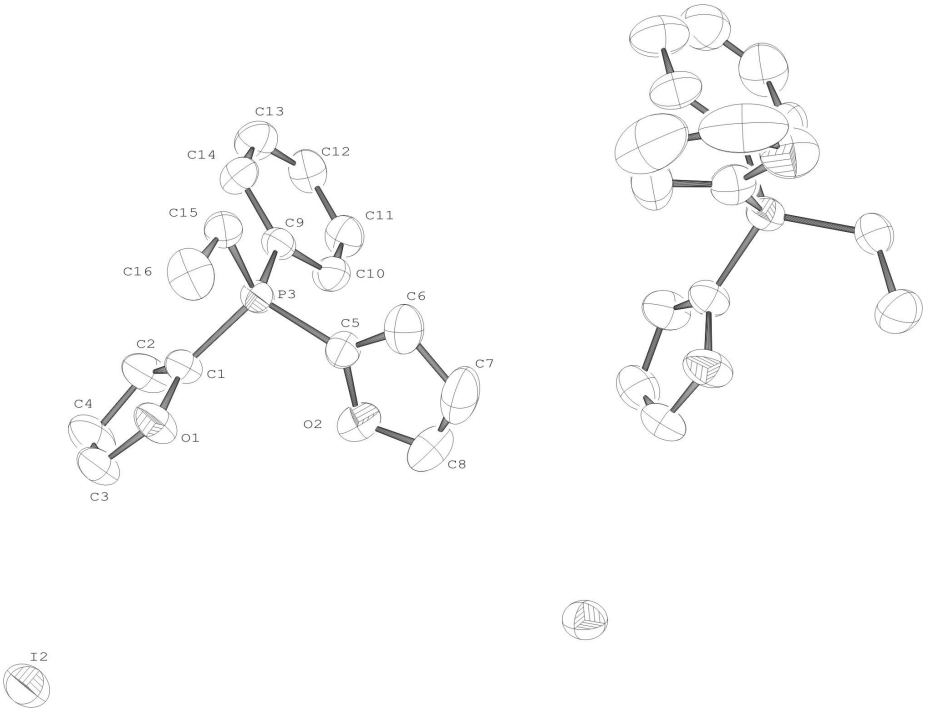


**Figure b**. Crystal structure of ethylbis(2-furyl)phenylphosphonium iodide **2c**.

Again two molecules are present in the unit cell, the crystal has an orthorombic crystal system with a Pca2 (1) space group. Since the thermal ellipsoids are smaller in the left structure, these coordinates were used for our calculations.

c) graphical representation of the shielding tensor

In figure c the orientation of the $^{31}$P-NMR main axis shielding components calculated with the 6-311G(d,p) basis set within the crystal structure of the ethyltriphenylphosphonium cation **2a** is shown.

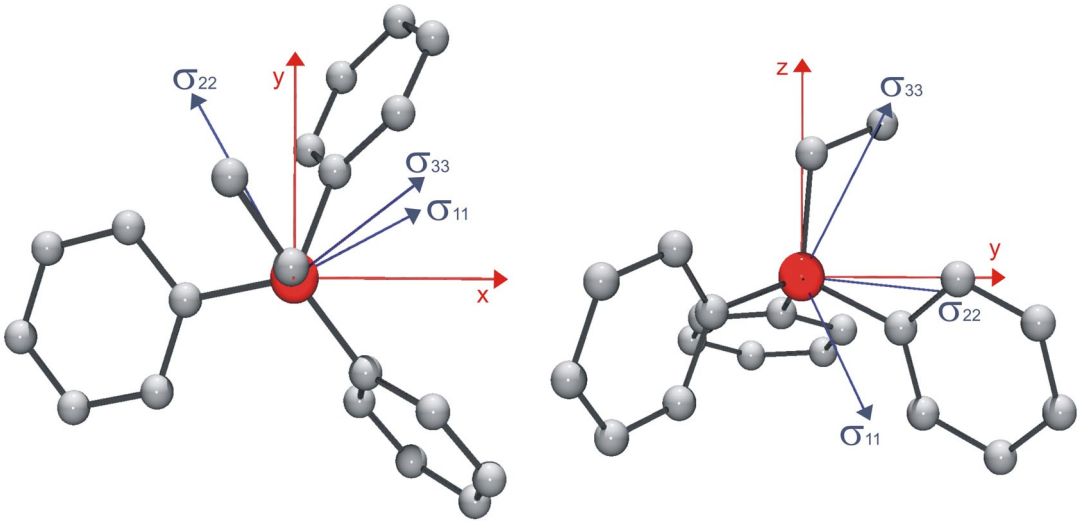


**Figure c**. Graphical representation of the main axis shielding components within the crystal structure of ethyltriphenylphosphonium cation **2a**. Left: View in direction of the negative z-achsis. Right: View in direction of the negative x-axis of the molecule coordinate system.

In figure d the orientation of the $^{31}$P-NMR main axis shielding components calculated with the 6-311G(d,p) basis set within the crystal structure of the ethyl(2-furyl)diphenyl-phosphonium iodide **2b** is shown.

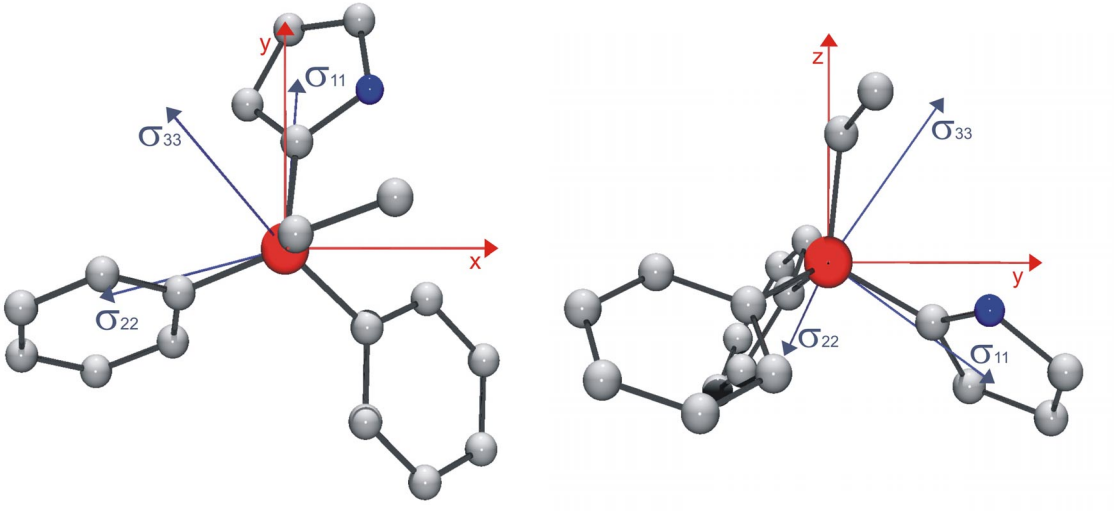


**Figure d**. Graphical representation of the main axis shielding components within the crystal structure of ethyl(2-furyl)diphenylphosphonium iodide **2b**. Left: View in direction of the negative z-achsis. Right: View in direction of the negative x-axis of the molecule coordinate system.

In figure e the orientation of the $^{31}$P-NMR main axis shielding components calculated with the 6-311G(d,p) basis set within the crystal structure of the ethylbis(2-furyl)phenylphosphonium iodide **2c** is shown.

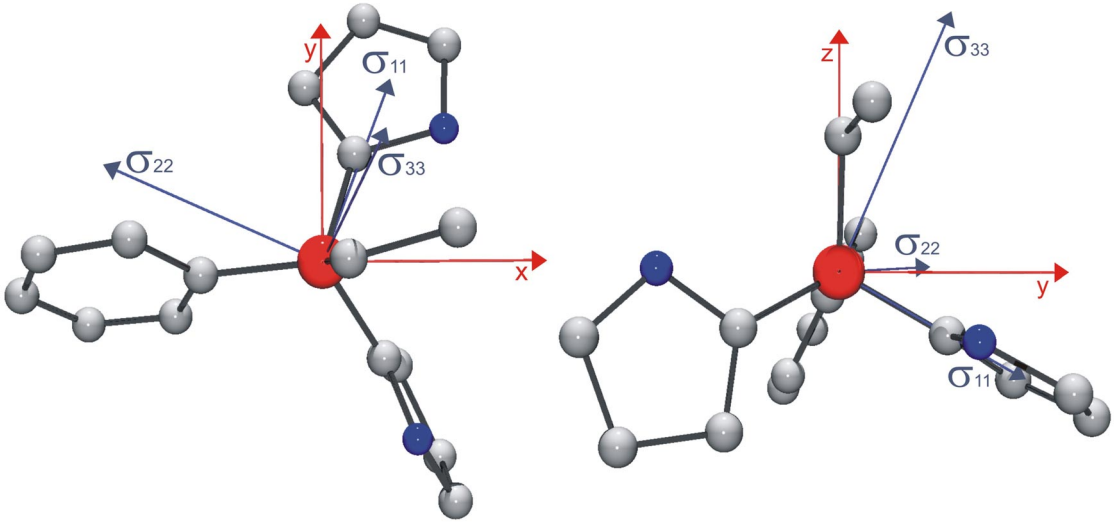


**Figure e**. Graphical representation of the main axis shielding components within the crystal structure of ethylbis(2-furyl)phenylphosphonium iodide **2c**. Left: View in direction of the negative z-achsis. Right: View in direction of the negative x-axis of the molecule coordinate system.

d) chemical shift tensor values obtained for the 6-311G(d,p) and G3large basis set

In table e the chemical shift tensor values as calculated with the 6-311G(d,p) basis set are shown.

| | $\delta_{11,g}$ [ppm] | $\delta_{11,s}$ [ppm] | $\delta_{22,g}$ [ppm] | $\delta_{22,s}$ [ppm] | $\delta_{33,g}$ [ppm] | $\delta_{33,s}$ [ppm] |
|---|---|---|---|---|---|---|
| $EtP^+Ph_3$ **2a** | 55.5 | 42.7 | 42.3 | 30.9 | 24.5 | 7.1 |
| $EtP^+Ph_2Fu$ **2b** | 47.7 | 39.2 | 21.4 | 14.7 | 5.5 | -5.0 |
| $EtP^+PhFu_2$ **2c** | 41.2 | 34.2 | 17.9 | 14.7 | -35.6 | -35.7 |
| $EtP^+Fu_3$ **2d** | 28.8 | 24.8 | -2.5 | -5.0 | -38.6 | -48.6 |
| $EtP^+Fu_3$ $Cl^-$ | 33.3 | | 3.0 | | -39.5 | |

**Table e**. The calculated (6-311G(d,p)) main axis components of the chemical shift tensor in the gas phase $\delta_{11,g}$, $\delta_{22,g}$, $\delta_{33,g}$ together with the experimental values $\delta_{11,s}$ to $\delta_{33,s}$ determined by $^{31}$P-MAS-NMR.

In table f the same results calculated with the G3large basis set are shown.

| | $\delta_{11,g}$ [ppm] | $\delta_{11,s}$ [ppm] | $\delta_{22,g}$ [ppm] | $\delta_{22,s}$ [ppm] | $\delta_{33,g}$ [ppm] | $\delta_{33,s}$ [ppm] |
|---|---|---|---|---|---|---|
| $EtP^{+}Ph_3$ **2a** | 78.7 | 42.7 | 64.1 | 30.9 | 44.4 | 7.1 |
| $EtP^{+}Ph_2Fu$ **2b** | 71.5 | 39.2 | 44.7 | 14.7 | 26.5 | -5.0 |
| $EtP^{+}PhFu_2$ **2c** | 65.8 | 34.2 | 45.2 | 14.7 | -10.3 | -35.7 |
| $EtP^{+}Fu_3$ **2d** | 52.8 | 24.8 | 22.2 | -5.0 | -17.1 | -48.6 |
| $EtP^{+}Fu_3$ $Cl^{-}$ | 57.8 | | 27.4 | | -18.5 | |

**Table f**. The calculated (G3large) main axis components of the chemical shift tensor in the gas phase $\delta_{11,g}$, $\delta_{22,g}$, $\delta_{33,g}$ together with the experimental values $\delta_{11,s}$ to $\delta_{33,s}$ determined by $^{31}$P-MAS-NMR.